High-resolution intra-urban assessments of future heat events and heat waves for the city of Augsburg, Germany

Christian Merkenschlager, Elke Hertig, Jonathan Simon, Christoph Beck

Angaben zur Veröffentlichung / Publication details:

Merkenschlager, Christian, Elke Hertig, Jonathan Simon, and Christoph Beck. 2023. "High-resolution intra-urban assessments of future heat events and heat waves for the city of Augsburg, Germany." *Urban Climate* 49: 101472. https://doi.org/10.1016/j.uclim.2023.101472.

High-resolution intra-urban assessments of future heat events and heat waves for the city of Augsburg, Germany

Christian Merkenschlager [a,b,*], Elke Hertig [b], Jonathan Simon [a], Christoph Beck [a]

[a] *Institute of Geography, University of Augsburg, Alter Postweg 118, 86159 Augsburg, Germany*
[b] *Faculty of Medicine, University of Augsburg, Werner-von-Siemens-Str. 6, 86159 Augsburg, Germany*

1. Introduction

Due to the expected climate change forced by the anthropogenic greenhouse gas emissions, the global temperature will increase by up to 1 °C–5.7 °C until the end of the 21st century compared to the pre-industrial area. Without significant emission cuts within the next decades, an increase of more than 2 °C is more than likely (IPCC, 2021). Thus, more regions of the world will be affected by extreme air temperatures and prolonged heat waves leading to increasing numbers of deaths or heat-related diseases like heat stroke, heat exhaustion, heat syncope and heat cramps (Kilbourne, 1997). Especially cities will become climate change hot spots since air temperatures within urban agglomerations are significantly higher than in its rural surroundings. Besides air temperature increase, the urban population is expected to increase up to nearly 70% of the global population until the mid of the 21st century (IPCC, 2021) and, thus, more and more people will be affected by heat-related diseases. But heat is not equally distributed within urban areas. Local air temperature patterns can be modified by local-specific characteristics like fraction of green space or sealed areas, distance to dense urban areas or sky view factor (Oke et al., 2017). Thus, in order to assess high-resolution intra-urban air temperature extremes and heat events, these factors should also be taken into account.

* Corresponding author at: Institute of Geography, University of Augsburg, Alter Postweg 118, 86159 Augsburg, Germany.
E-mail address: christian.merkenschlager@med.uni-augsburg.de (C. Merkenschlager).

The fact that urban areas are warmer than its rural surroundings was first mentioned by Howard (1818). Since then, many publications were dedicated to the so-called urban heat island effect (Oke, 1987). The UHI summarizes physical characteristics of specific surfaces. For example, buildings or sealed areas exhibit a higher heat storage capacity so that they can store (day) or emit (night) more heat than natural surfaces (Chudnovsky et al., 2004). In contrast, green spaces exhibit higher soil moisture and plants and, thus, a higher evapotranspiration which ensures a cooling effect for its surrounding (Jusuf et al., 2007). The canopy layer UHI reaches its maximum at nighttime under cloudless and calm weather conditions and can be over 10 °C in major metropolises (Rizwan et al., 2008). An air temperature up to 10 °C higher within urban areas also naturally affects the number of extreme temperature events and the number and duration of heat events. In the present study, we analyzed the future development of heat events within the medium-sized city of Augsburg (Bavaria, Southern Germany) under consideration of moderate (RCP4.5) and a strong (RCP8.5) Representative Concentration Pathway.

Most of the studies which deal with the assessment of future climate change within urban areas are based on Regional Climate Models (RCMs). The information derived from the dynamical downscaling process are then implemented in a statistical model or used to determine the boundary conditions of an urban climate model (e.g., Lauwaet et al., 2016; Hamdi et al., 2014). However, RCMs are accompanied by a high amount of computing effort and memory capacity so that the dynamical downscaling represents a cost-intensive and time-consuming method (Teutschbein et al., 2011). Statistical methods like (urban) weather generators (e.g., Salvati et al., 2017; Le Bras and Masson, 2015; Bueno et al., 2013), regression models (MLR e.g., Straub et al., 2019; Ketterer and Matzarakis, 2015), regression trees (e.g., Makido et al., 2016) or random forests (e.g., Ho et al., 2014) are also applied within urban climate science but all mentioned studies do not deal with projections of urban climate change. Studies which applied statistical methods for projections of urban heat events or the UHI either exhibit a too sparse resolution to identify intra-district hot spots (e.g., Bartos and Chester, 2014) or the spatial distribution model for temperatures is only based on a little number of stations within the city (e.g., Ortiz et al., 2019). Thus, the authors of the latter study also applied dynamical downscaling and came to the conclusion that dynamical

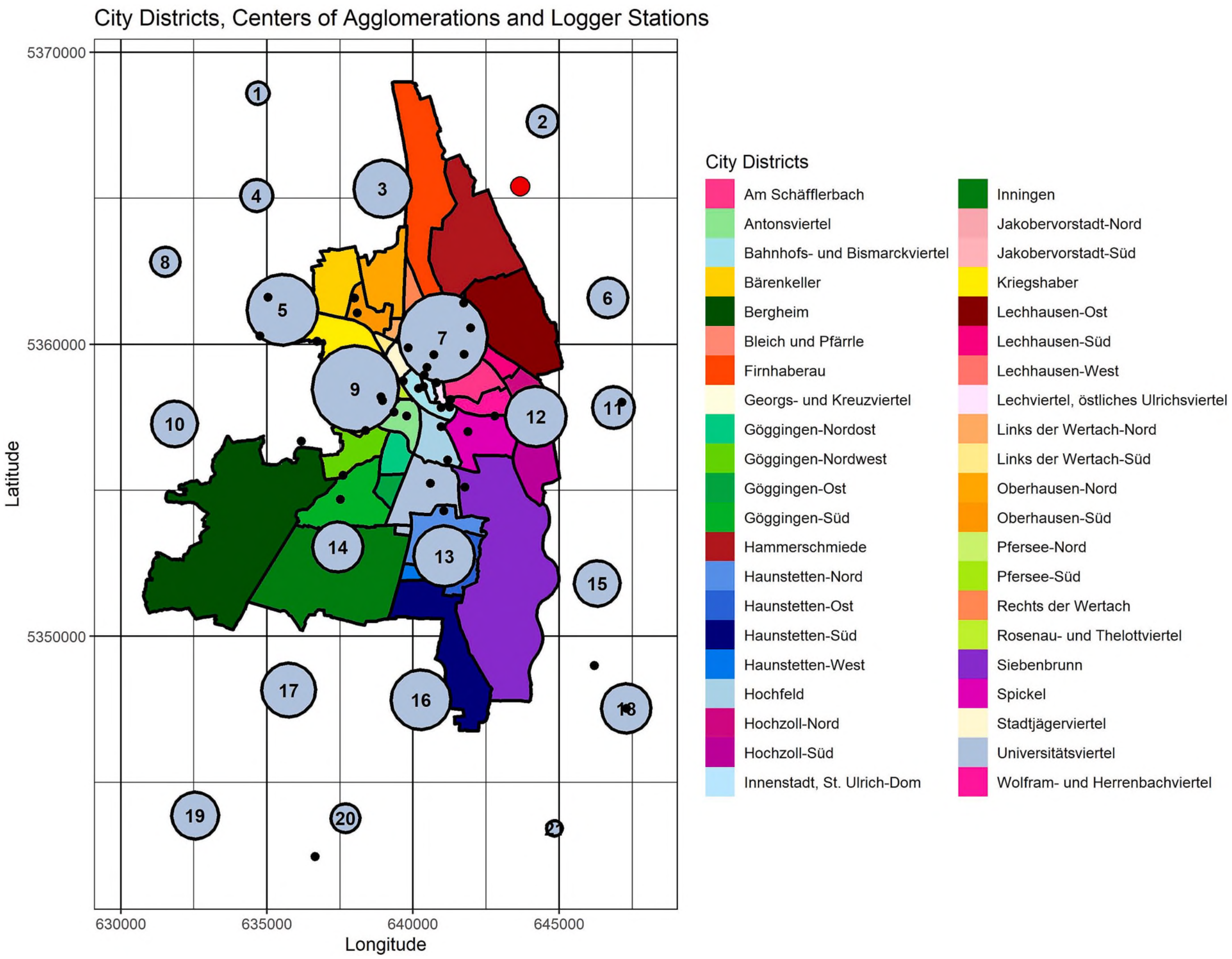

Fig. 1. City districts (colored areas), urban centers of agglomeration (numbered circles) and logger stations (black dots) within the study area of Augsburg, Bavaria. The meteorological station of Augsburg-Mühlhausen (DWD) is represented by a red dot. (For interpretation of the references to colour in this figure legend, the reader is referred to the web version of this article.)

outperforms statistical downscaling. Since the quality of the statistical transfer function highly depends on quality and quantity of available data (Teutschbein et al., 2011), we used a dense urban meteorological network with 38 quality checked logger stations over an area of 146.9km^2 for model setup in order to overcome this lack of skill. If the quality and quantity of the data is high, the results of statistical approaches are indeed meaningful and comparable to dynamical downscaling approaches (Hertig and Jacobeit, 2008). Furthermore, statistical downscaling is bounded to specific framework conditions. On the one hand, the relationship between predictor and predictand established within the reference period should also be stable under climate change conditions. On the other hand, a thorough selection of predictors should be conducted (Gutierrez et al., 2013). In our study, the latter is given by a selection process based on cross-validation of different predictor combinations whereas the former can only be assumed to be valid under climate change conditions (Diaz-Nieto and Wilby, 2005).

The present study provides a comprehensive analysis of heat events for a medium-sized city in central Europe. The study is based on novel statistical downscaling techniques which aim to reduce computational costs without losing model skill in comparison to other established analog models. Furthermore, the assessments of the spatial distribution of temperatures are based on a dense meteorological network which allows for precise temperature assessments on a very high resolution. Thus, the study provides a significant contribution towards the understanding of heat extremes within urban areas under climate change conditions. Detailed assessments of intra-urban heat events can help urban planners to identify urban climate change hot spots. Thus, countermeasures like renaturation of sealed areas can be implemented immediately in order to reduce the impacts of climate change. Furthermore, public health services can precisely establish a range of measures early, including management of chronic diseases or institutional care of elderly and vulnerable people to reduce health impacts (Kovats and Hajat, 2008).

In section 2, the data which were used in this study are described. The linear regression model and its modifications for assessing the spatial temperature distribution are presented in section 3. The results for absolute and relative temperature extremes are summarized in section 4. A discussion about the results is given in section 5. Finally, the conclusions in section 6 summarizes the present study and highlights the major findings.

2. Data

Since analysis are performed with respect to warm temperature extremes, all data are limited to the extended summer season from May, 1st to September, 30th.

2.1. Study area

The study area is limited to the official urban area of the city of Augsburg (296.582 inhabitants, Stadt Augsburg 2020). Augsburg is located in Bavaria, Southern Germany (10.90°E, 48.37°N), between 444 m (Firnhaberau, North) and 562 m (Bergheim, Southwest) a.s.l., covers an area of 146.86 km^2 and its maximum extension is 22.3 km (North-South) and 14.7 km (East-West), respectively. The city is divided into 42 city districts (Fig. 1) with large forest areas in the south-eastern and south-western parts and two rivers which cross the city area from south to north. Overall, 50% of the city area is covered by agricultural land or forests, 37.4% by buildings or infrastructure facilities and 6.6% by water bodies (Amt für Statistik und Stadforschung, Stadt Augsburg, 2017).

The weather of Augsburg is determined by a warm temperate climate with humid conditions throughout the year (Kottek et al., 2006) and thus belongs to the Cfb type of the Köppen-Geiger climate classification. The long-term mean of the annual air temperatures is 8.5 °C with highest monthly mean temperatures in July (18.1 °C). The mean annual rainfall sum is 767 mm and the main wind direction is southwest (Beck et al., 2018).

2.2. Long-term weather station

Daily meteorological data of air temperature 2 m above ground (TMIN, TMEAN and TMAX), relative humidity (RHUM), wind speed (WSPD) and direction (WDIR), cloud cover (CC) and sunshine duration (SD), sea level (SLP) and vapor pressure (VAPOR) from the Augsburg-Mühlhausen weather station (elevation: 461.4 m; 10.9420°E, 48.4254°N) operated by the German Weather Service (DWD Climate Data Center Deutscher Wetterdienst, 2019) were included in the analysis. The station data comprises daily data from 1950 to present and is situated north of Augsburg near the airport of Mühlhausen. The station is mainly surrounded by agricultural land (Straub et al., 2019). In Fig. 1, the Augsburg-Mühlhausen weather station is represented by a red dot.

2.3. Urban meteorological network

The urban meteorological network is based on 80 HOBO pro v2 U23–001 data loggers which measure air temperature and relative humidity with 4 min temporal resolution (Onset, 2010). The data loggers were set up in a cooperative effort of the Helmholtz Zentrum München (German Research Center for Environmental Health, Institute of Epidemiology, Environmental Risks) and the University of Augsburg (Institute of Geography, Physical Geography and Quantitative Methods) in December 2012. Information about the accuracy of the sensors, the methods which were used for the quality check and site-specific information are described in detail in Beck et al. (2018). For the present study, data for the extended summer season for the period 2013–2018 were used. With respect to completeness, a day was assumed to be complete when 80% of the daily data were available. Furthermore, a station was assumed to be complete when the logger time series contains at least 80% of the days of the extended summer season. Overall, 38 stations meet the given conditions. The locations of the logger sites are given in Fig. 1 (black dots).

2.4. Reanalysis data

The prevailing circulation is represented by the geopotential heights on the 850 hPa level (HGT.0850) of the ERA5 reanalysis data set provided by the European Centre for Medium-Range Weather Forecasts (Copernicus Climate Change Service (C3S), 2017). In order to represent the circulation similar to the highest resolution of the Generalized Circulation Models (GCMs) of the Coupled Model Intercomparison Project- Phase 5 (CMIP5), the data were downloaded on a 0.75°x0.75° grid, covering an area from 0.25° to 19.75°E and 40.0° to 59.5°N (27 × 27 grid, 729 grid boxes). Furthermore, daily minimum, mean and maximum temperatures at two meters above ground (T2M) for the grid box containing Augsburg-Mühlhausen weather station and its eight surrounding grid boxes were taken into account for the analysis. All reanalysis data sets were trimmed to the extended summer season of the period 1979–2018.

2.5. Generalized circulation models (GCMs)

For projections, analyses are based on five model runs of three different GCMs which cover the period from 1950 to 2100. According to the reanalysis data, the same circulation and temperature data for the Representative Concentration Pathways (RCP) with a radiative forcing of 4.5 W/m^2 and 8.5 W/m^2 were downloaded for the ACCESS1–0 (RUN 1) model provided by the Australian Community Climate and Earth System Simulator, Australia, the CNRM-CM5 (RUN 1) model of the Centre National de Recherches Meteorologiques, France, and the MPI-ESM-LR (RUN 1–3) of the Max-Planck-Institute, Germany. All data sets were interpolated on the same regular grid provided by the reanalysis data set and adjusted to the extended summer season. Analyses have shown that, in comparison with the reanalysis data, all model runs exhibit rather similar variances and seasonal mean values for the period 1979–2018 and, thus, are suitable for temperature projections for the study area (Supplementary S1.2, S2.2). This is also supported by Brands (2013) who analyzed how well earth system models of the CMIP5 represent recent climate conditions in Europe.

2.6. Spatial characteristics

In the present study, the spatial characteristics of the urban area of Augsburg are described by four different data sets. The European

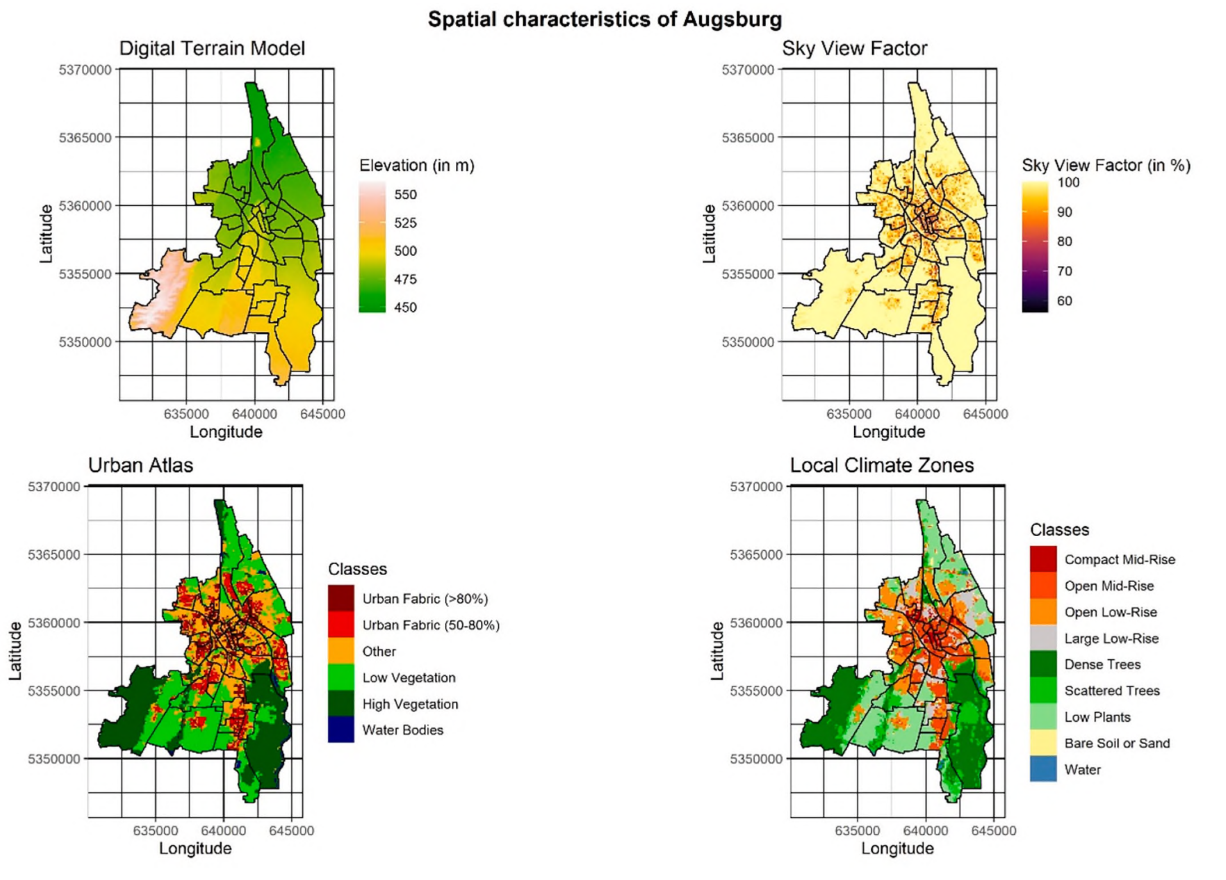

Fig. 2. Spatial characteristics of Augsburg. The figures represent the elevation (top left), the sky view factor (top right), the modified urban atlas classes (bottom left) and the local climate zones (bottom right).

Urban Atlas (UA, EEA, 2010) as well as the Local Climate Zones (LCZ, Bechtel and Daneke, 2012; Bechtel et al., 2015) determined for Augsburg (Beck et al., 2018) represent the land use characteristics within the city of Augsburg. Since the UA contains more than 20 different classes, various classes were summarized according to the fraction of sealed or green space areas and building heights. Overall, six different classes of the modified UA were taken into account for further analysis. Furthermore, the UA data set was used to determine urban agglomeration centers (UACs). Here, UACs represent contiguous areas of dense urban structures with only little green areas and a high proportion of sealed areas. A mean shift cluster algorithm established by Cheng (1995) was applied to the categories with continuous or discontinuous urban fabric over 50%. The assigned grid boxes were then used to determine circular UACs. Overall, 21 UACs were obtained with areas from 0.22 to 7.25km^2. The UACs are numbered and displayed in Fig. 1 as slate blue shaded circles and the area of the circles corresponds to the area of the UAC. A larger domain was chosen for the calculation of the UACs since nearby UACs outside the city may also affect loggers or grid boxes close to the city borders. Furthermore, wind speed and direction were also considered to assess the degree of influence of the UACs. In particular, the effect of densely built-up areas (e.g., local UHIs) on surroundings is slightly shifted by wind speed and direction. A digital terrain model (DGM) and the sky view factor (SVF) derived from data of the Landesamt für Digitalisierung, Breitband und Vermessung (LDBV, 2017) were taken into account in order to consider elevation and site-specific shadowing effects caused by buildings. All data sets were interpolated on a regular grid of 100 m × 100 m resulting in 14,674 grid boxes (Fig. 2).

3. Method

3.1. Projections for Augsburg-Mühlhausen

The projections for Augsburg-Mühlhausen were performed by an analog method based on the normal vector (NVEC) of the circulation patterns. For each day of the extended summer season of the GCM model runs, an analog day was selected from the ERA5 reanalysis data set. Prior to this, all temperature data sets (reanalysis, GCMs) were bias corrected and detrended using the Augsburg-Mühlhausen temperature time series. A detailed description of bias correction and detrending as well as the analog method is given in Merkenschlager et al. (2021).

The analog method is divided into three steps: preselection – first level of analogy – second level of analogy. The setup for the analog method corresponds to the Q90 + T2M described in Merkenschlager et al. (2021). This means the initial subsample of potential analog days is limited to ±15 days of the day of interest and equal exceedances of the 90th quantile (Q90). By means of the NVEC analog method, distances between points (day of interest → analog days) within an artificial coordinate system defined by the mean of the geopotential heights and the inclination and direction of the corresponding normal vector were calculated (first level of analogy). Subsequently, the 5% of analog days which exhibit the least distances between the points were considered for the final analog selection. The second level of analogy is then performed by means of the mean Root Mean Square Error (RMSE) of the gridded temperature data (T2M). The day of the subsample which exhibits the lowest mean RMSE was defined as analog day. Since analysis aims on temperature extremes and heat events, only one analog day was chosen instead of an analog ensemble in order to avoid the flattening of the tails of the temperature distribution. The variables given by Augsburg-Mühlhausen and the circulation pattern of ERA5 finally represent the analog day for the respective day of interest of the GCM. Thus, for each model run of the GCM we obtain a time series of variables represented by Augsburg-Mühlhausen or ERA5, respectively, for the period 1950–2100. Subsequently, the trends of the respective model run of the GCMs were added to the detrended temperature time series of Augsburg-Mühlhausen, again. Since historical periods and scenarios were jointly analyzed (historical+RCP4.5, historical+RCP8.5), small differences within the historical periods can occur. For simplicity, the results of the historical periods were averaged and subsequently named historical period. Thus, we obtain time series of meteorological variables based on the observation but under consideration of climate change represented by the GCMs.

3.2. Spatial extrapolation of temperatures

The analog time series of Augsburg-Mühlhausen and ERA5 are now used as temporal predictors for a multiple linear regression (MLR) to extrapolate temperatures to the study area. The variables T2M, RHUM, SD, CC, SLP and VAPOR represent the temporal predictors of Augsburg-Mühlhausen. The circulation represented by ERA5 were subjected to a t-mode principal component analysis (PCA, Preisendorfer, 1988). Subsequently, the time series of the PC-loadings derived from the t-mode PCA (S1.1) were also taken into account as temporal predictors. The categorial variables of UA and LCZ as well as the SVF and the DGM represent the spatial predictor variables. Since the UHI affects temperature behavior within each UAC and its surroundings, a weighted distance model was established in order to assess the influence of each UAC on each logger station or grid box, respectively. For this purpose, the physical locations of the logger stations or grid boxes with respect to the UACs as well as WDIR and WSPD of the Augsburg-Mühlhausen analog time series were used. The temperature time series of the 38 logger stations were taken into account as predictands for model calibration and validation.

3.2.1. Weighted distance

When the absolute distances were considered for model calibration a small number of logger stations at the edge of the study area led to unrealistic temperature values when the established model was applied to the grid boxes. Thus, weighted distances were used. The calculation of the weighted distances is based on a simple model which considers whether or not the logger stations (grid boxes) lie within a UAC, and, if not, depending on the wind direction, if the station or grid box is in the catchment area of the UAC. The size of the

UAC and the wind speed was used to determine the range of influence of the respective UAC. The higher the wind speed and the larger the UAC, the larger the range of influence. If the logger station or grid box lies exactly at the outer edge of the center, the weighted distance is 1, whereas logger stations or grid boxes within (outside) the center exhibit higher (lower) values. A summary of the weighted distance model is given in S3.

3.2.2. Spatial model

For each temperature variable (TMIN, TMEAN and TMAX) a specific MLR model was established for all days representing one of the four leading principal components (PCs) of the t-mode PCA. Since the sample size for the last two PCs is too small for cross validation, days which exhibit highest loadings on these two PCs were excluded from temperature assessments. Thus, twelve models were established to assess minimum, mean and maximum temperatures for the four remaining PCs. Overall, with respect to missing data or assignment to one of the last two PCs, temperature assessments could be conducted for 98.3% of all days of the time series. The spatial model was calibrated by means of the logger time series for the extended summer season of the period 2013–2018. For cross-validation, the Mean Square Error Skill Score (MSESS) was used to assess the skill of the temperature assessments. As reference, a model which only considers the temperatures of Augsburg-Mühlhausen as predictor variable was taken into account. The MSESS is given in S2.3 and indicates how much better the established model is in comparison to the reference. The cross-validation process is based on leave one out, i.e., the temperatures from one year of one station were always assessed by means of the model established by means of the remaining stations and years. The skill is defined by the exceedance of the MSESS of the established over the reference model.

The elimination criterion (EC) for the predictors is based on the MSESS and depends on the predictor variable. The temperature variable given by the analog time series of Augsburg-Mühlhausen was always considered within the model setup. The EC for the remaining temporal variables were set to 0.05. First, the linear regression was performed under consideration of all temporal predictors and a reference MSESS ($MSESS_{REF}$) was calculated. Subsequently, a backward oriented stepwise elimination of predictors was performed i.e., regressions were performed by leave-one-out predictor. If the MSESS of the worst predictor declines (exceeds) the threshold of $MSESS_{REF}$ - EC the respective temporal variable was taken into account (eliminated) for model setup. If the new MSESS even exceeds the $MSESS_{REF}$ the new MSESS replaces the $MSESS_{REF}$. Furthermore, the circulation patterns of ERA5 represented by their respective PC-loadings were considered as a whole, i.e., if the MSESS exceeds (falls below) the $MSESS_{REF}$ – EC, all PCs were removed (taken into account). To obtain a higher spatial differentiation of the temperatures, the EC for spatial predictors was set to 0, so that any improvement of the MSESS has led to the consideration of the respective spatial predictor. In contrast to the PCs, each weighted distance to the UAC was investigated, separately. Thus, a UAC was eliminated when its consideration results in a decline of the MSESS.

3.3. Definition of heat or anomaly waves

Since there is no universal definition of heat extremes or waves (Perkins, 2015), analysis of extremes was performed by means of absolute as well as relative thresholds. Relative thresholds are commonly defined as the daily (calendar-day) 90th quantile (Q90) of the respective temperature variable (e.g., Meehl and Tebaldi, 2004), whereas absolute thresholds are defined by fixed temperature values (e.g., Zhao et al., 2018). Even the delineation of the duration for heat waves is not uniform (e.g., 6 consecutive days Fischer and Schär, 2010; 3 consecutive days Vautard et al., 2013), but most studies define a heat wave by three or more consecutive days exceeding a certain threshold since mortality increases dramatically when heat events last more than 2 days (Pantavou et al., 2008). In this study, we apply thresholds on all temperature variables and, thus, the definition of heat waves, too. The relative threshold of the respective temperature is based on the exceedance of the daily Q90, whereas the absolute thresholds were set to 20 °C for TMIN (tropical night), 25 °C for TMEAN and 30 °C for TMAX (hot day). If a day exceeds at least two of three thresholds, the day was defined as positive anomaly day (PAD) or heat day (HD), respectively. An event comprises each kind of consecutive PADs or HDs. Thus, a heat event (HE) or positive anomaly event (PAE) can last only one day as well as more than ten days. In accordance with most studies, the minimum duration for a heat wave (HW) or positive anomaly wave (PAW), respectively, was set to at least three days. Furthermore, HW and PAW were categorized by duration so that short waves last 3–5 days, medium waves 6–9 days and long waves ten or more days.

4. Results

4.1. Model performance

The skill of the analog model (NVEC) used in this study is described in detail in Merkenschlager et al. (2021). It shows that the applied method can keep up with existing analog techniques and provides good skills. The highest skills were obtained by using HGT.0850 of the ERA5 data set for the first level of analogy as well as for the spatial extrapolation of the temperatures.

Cross-validation for the spatial temperature model shows that the method is appropriate to assess temperatures within the study area. For all stations and years, the MSESS was calculated by means of the regression models and a model based on temperature (reference), only. The MSESS ranges from approximately 0.1 to 0.8 indicating an improvement over the reference for all stations and years. Thus, the final spatial regression models were established under consideration of all stations and years. The final predictor sets for each temperature variable and PC as well as the MSESS and the Root Mean Square Error (RMSE) from cross-validation are presented in S2.3.

For TMIN, all predictor sets contain the temporal predictors T2M, RHUM, VAPOR of Augsburg-Mühlhausen and the circulation patterns of ERA5, whereas CC, SLP and, to some extent, SD are redundant. In contrast, SD is part of all predictor sets of TMEAN whereas

RHUM is eliminated. The temporal predictor set of TMAX contains almost all temporal variables, only CC and SLP are eliminated for PC-1 and/or PC-2, respectively. LCZ and UA seem to be the most powerful spatial predictors, whereas SVF is only significant for TMIN and PC-4 of TMAX, and DGM data were only considered as predictor for two PCs (TMIN PC-1, TMEAN PC-4). The most important UAC for all MLR models is UAC-7 located in the city center of Augsburg, since only one model eliminates these UAC. Overall, the consideration of UACs improves the model skill (MSESS +0.0914 on average), only PC-4 of TMAX excludes the weighted distances within the model calibration process.

4.2. *Historical reference period of Augsburg-Mühlhausen*

The historical runs were jointly analyzed with the RCP scenarios. Thus, the following results contain historical periods for RCP4.5 and RCP8.5. As expected, differences between both historical periods of the RCPs are rather small (Fig. 3). Thus, the historical periods are averaged, and the following results are related to the historical period, only. Since all data sets only cover the years 1979–2005 within the historical period, analyses of the skill were limited to this period. Overall, the mean of the daily temperature variables of Augsburg-Mühlhausen were overestimated by the GCMs by 0.7 °C–2.1 °C with minor deviations for TMIN. Almost each model run of the GCMs exhibits a lower standard deviation with up to 0.92 °C for TMAX. The Box-Whisker-plots for the daily temperature values for both RCPs are presented in Fig. 3.

For all other temporal predictor variables, the Whisker-Boxplots are presented in S2.2. The figure shows that the distributions as well as the means of the daily values are well reproduced by the analog time series of the GCM model runs. Only the mean sunshine duration was slightly overestimated and, therefore, the cloud cover underestimated by the analog time series.

With respect to the circulation, the patterns of the analog time series approximately correspond to the patterns of the reanalysis data set. In general, the positive and negative modes of the first two PCs represent the dominant circulation patterns. Only the French model CNRM-CM5 clearly underestimates (overestimates) the likelihood of occurrence of PC-2 (PC-3), which leads to a changing order of the dominant PCs. Significant deviations can also be seen for PC-1 of the MPI-ESM-LR model run 3, since the positive mode was occurring 7.8% more frequently than within the ERA5 data set. For PC-4, only the analog time series of CNRM-CM5 captures that the positive mode occurs more frequently than the negative mode, whereas all other analog time series show the negative mode up to three times more frequently than during observation. The occurrence of circulation patterns for the different analog time series of the GCMs are presented in detail in S1.2.

With respect to the mean duration of PAEs, only ACCESS1.0 RUN1 assigns more days to events of 3–5 days than to events of less than three days (not shown). The only model which does not exhibit a PAE with a duration of more than ten days is MPI-ESM-LR RUN2. Overall, only CNRM-CM5 RUN1 (11.16 days) exhibits a smaller number of days exceeding two of three thresholds than the observation (12.26 days). With respect to HDs, CNRM-CM5 RUN1 (1.9 days) exhibits three times more HDs per year than the observation (0.63 days, not shown). Thus, for CNRM-CM5 the absolute (HD) and relative (PAE) thresholds show a contrary development. In accordance with the observation, the reanalysis and the models of MPI-ESM-LR exhibit less than one day per year which exceeds two of the three

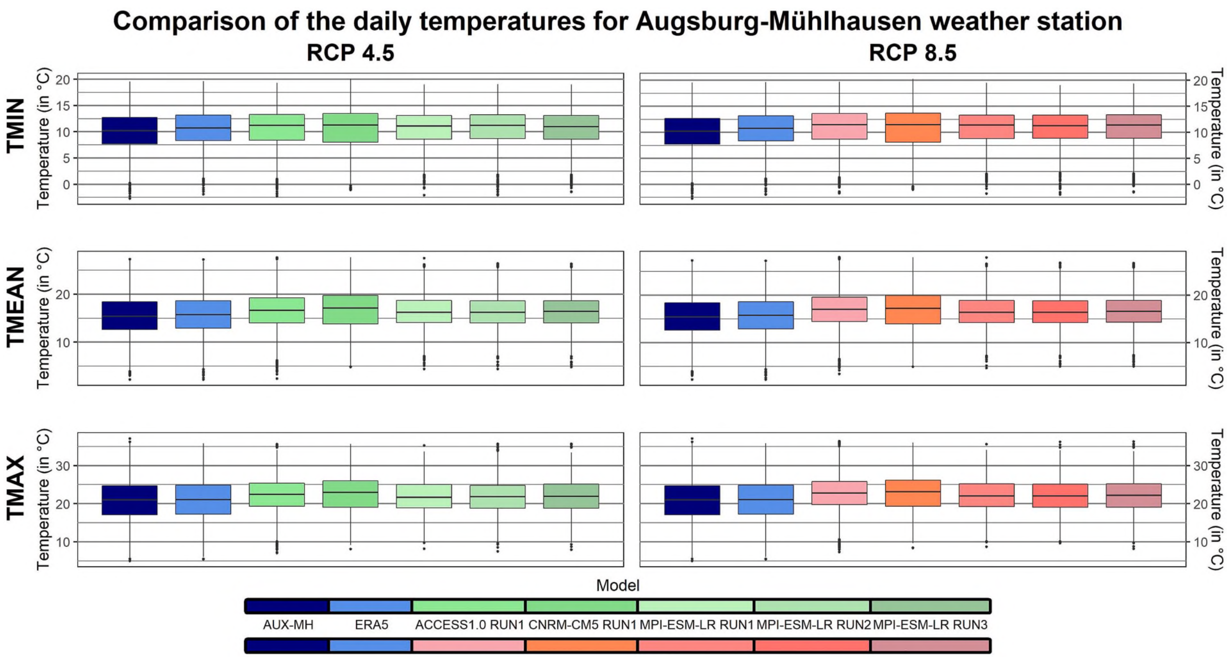

Fig. 3. Comparison of the daily temperatures for the period 1979–2005 for RCP4.5 (left) and RCP8.5 (right). The colors represent the observation (AUX-MH), reanalysis (ERA5) and different runs of the GCMs ACCESS1.0, CNRM-CM5 and MPI-ESM-LR.

temperature variables. However, some models show a different distribution with respect to the duration of HEs. HEs of more than six days do not occur within the observation but ERA5 and ACCESS1–0 RUN1 even exhibit HEs of more than 10 days. On average, all models exhibit less than one HE per year within the reference period and HEs of more than five days are very rare. Detailed information about the exceedance of thresholds by temperature are given in S2.4.

The mean heat day period (HDP) of the observation lasts from July, 18th to July, 26th and exhibits a mean duration of 9 days. The HDP is limited by the first and the last day of the year where a heat day occurs. Here, the first and last day are averaged over all years of the reference period which exhibit a HD. Years when no heat day occurs were eliminated. The number of years without any HD is given as second number in Fig. 4. Independent of model, more than half of the years of the reference period do not exhibit a HD. The figure also shows that only the HDP of ACCESS1–0 RUN1 is considerably earlier in the year and significantly longer than the HDP of the other models. In general, the HDP starts mid of July and ends in the late third of July or early third of August.

4.3. Projections for Augsburg-Mühlhausen

4.3.1. Temperature

In Fig. 5, the downscaled annual mean temperatures of Augsburg-Mühlhausen are given for all temperature variables. For comparison, observation (darkblue) and reanalysis (blue) data are also presented for the period 1979–2018. Under consideration of RCP4.5 (RCP8.5), the historical reference period (1970–2000) exhibits a mean temperature of 10.6 °C (10.8 °C) for TMIN, 16.3 °C (16.4 °C) for TMEAN and 21.9 °C (22.2 °C) for TMAX. For RCP4.5 the strongest increase with 1.1 °C for TMIN and TMEAN and 1.2 °C for TMAX can be observed for the early 21st century (period: 2010–2040). For the mid (2040–2070) and late (2070–2100) 21st century, the rate of temperature rise is steadily decreasing. In comparison with the historical reference period the temperatures for Augsburg-Mühlhausen are 2.2 °C–2.7 °C higher at the end of the 21st century. In contrast, under consideration of RCP8.5 the highest rate of temperature rise was projected for the late 21st century. Here, with respect to the previous period an increase in temperature of 1.9 °C–2.3 °C was projected, leading to temperatures of 4.3 °C–5.3 °C higher than within the historical period.

4.3.2. Positive anomalies

The rise in temperature within the 21st century leads to an increase of PADs and PAEs (Fig. 6). At the end of the 21st century, about 75% (50%) of all days exhibit at least one temperature variable which exceeds Q90 under consideration of RCP8.5 (RCP4.5), and over 60% (30%) are by definition PADs. While most of the PADs of the historical period are assigned to events of 1–2 days, a shift to longer lasting events occurs in the future periods. In period 2010–2040, most PADs are assigned to PAEs with a duration of 3–5 days and from the middle of the century on, PAEs of more than 10 days exhibit the largest number of days (2070–2100: 19.3 days in RCP4.5; 65.3 days in RCP8.5). Within the historical reference period, 5 PAEs per year can be observed and mostly exhibit a duration of 1–2 days (RCP4.5: 3.6; RCP8.5: 4.1 days). The likelihood of PAEs with more than 10 days exists but is almost zero. Throughout the 21st century,

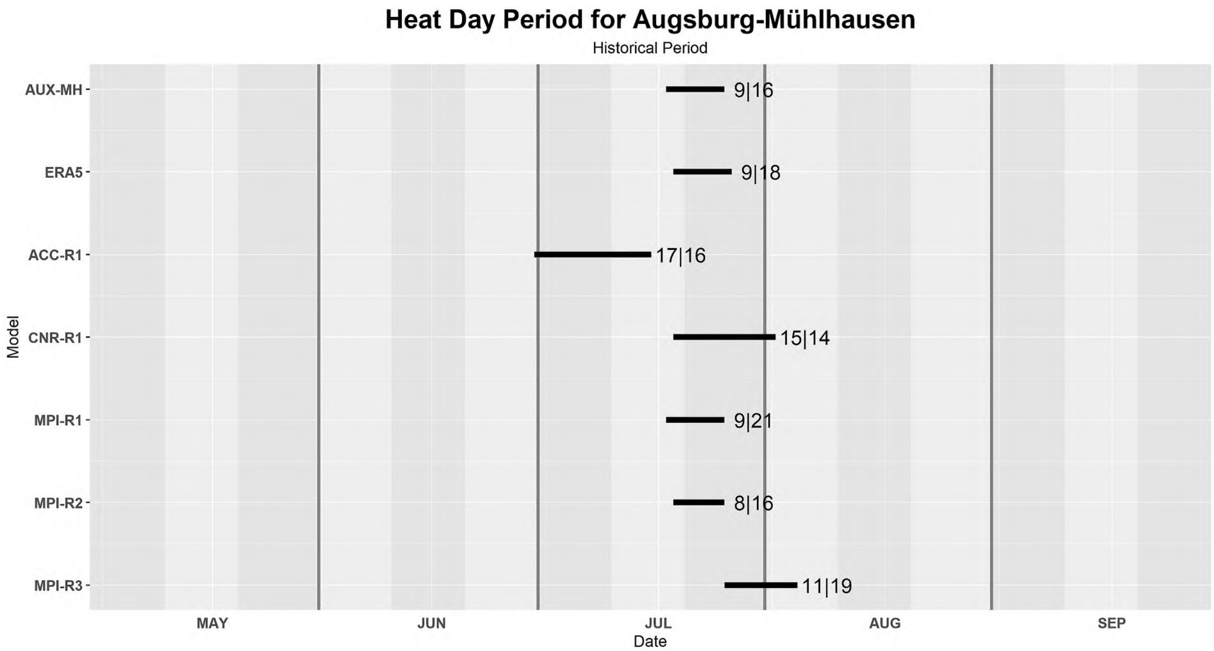

Fig. 4. Temporal classification of the heat day period within the historical period (1979–2005) for the observation, reanalysis and the different model runs. The line depicts the mean heat period (period between first and last heat day of the year) where heat days occur. The first number gives the mean duration of the heat period in days, the second number the number of years without a heat day.

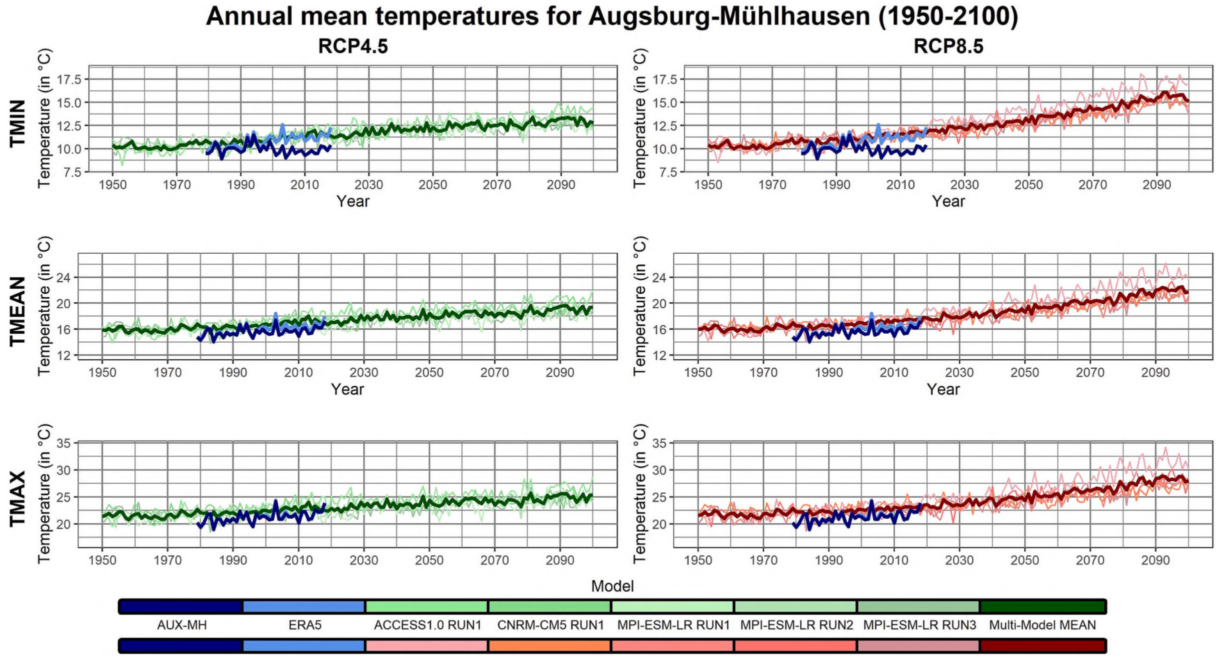

Fig. 5. Projections of annual mean temperatures of TMIN, TMEAN and TMAX for Augsburg-Mühlhausen under consideration of RCP4.5 (left) and RCP8.5 (right). Observation and reanalysis are depicted in blue; the model runs of GCMs in light green or red solid thin lines. The multi-model mean is represented by bold dark colored lines. (For interpretation of the references to colour in this figure legend, the reader is referred to the web version of this article.)

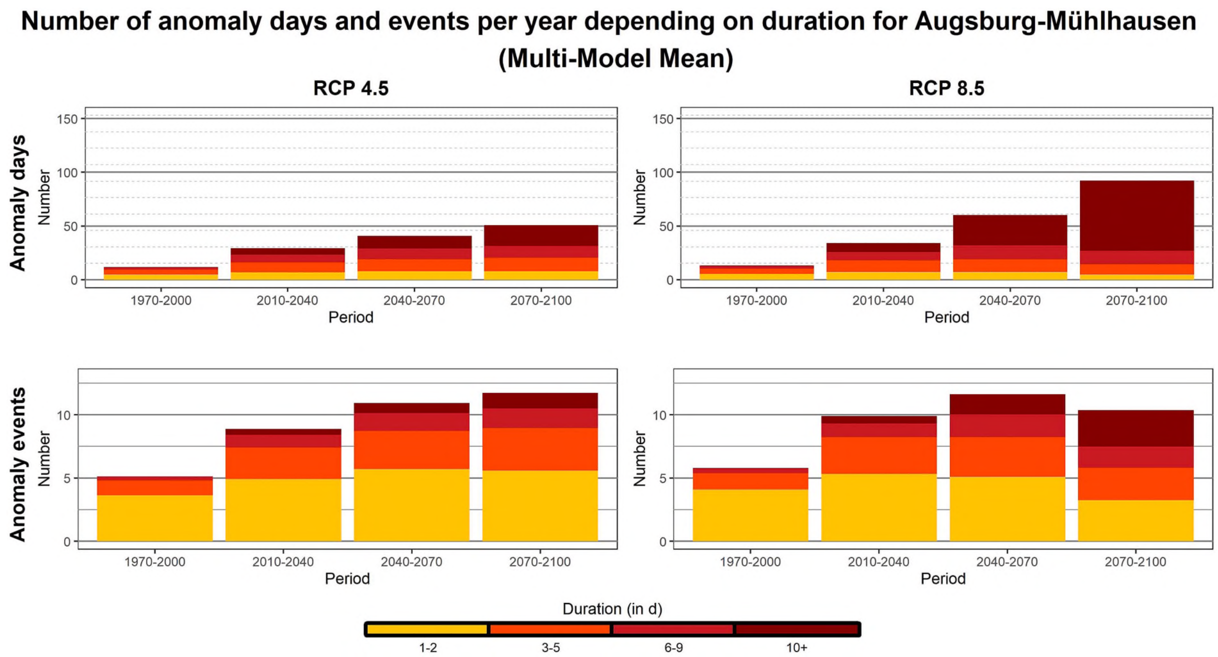

Fig. 6. Number of positive anomaly days (PADs, top) and events (PAEs, bottom) with respect to the length of an event for RCP4.5 (left) and RCP8.5 (right). Solid lines in the upper figures represent the absolute numbers, dashed lines the relative number in percent in steps of 10.

PAE of 1–2 days are noted most frequently but under consideration of RCP8.5 (RCP4.5) the number decreases in the middle (end) of the 21st century. A decrease can also be observed for PAEs with 3–5 and 6–9 days at the end of the 21st century for RCP8.5, whereas an intensified increase of PAEs of 10 or more days (10+ PAE) takes place. In period 2070–2100, almost 3 PAEs of more than 10 days can be expected per year. In comparison, a 10+ PAE within the historical period can be observed every 10 years. Overall, at the end of the 21st century the number of PAEs decreases in favor of longer lasting events, since shorter events are merged to one longer event. For RCP4.5, a steady increase of PAEs with more than 3 days can be observed for the 21st century and, thus, the number of days as well as the number of events increase throughout the 21st century.

In Fig. 7, time series based on 31 year periods are depicted for the number of anomaly days and waves and the mean and maximum duration of anomaly events. It shows that the number of PAWs is more than four times higher at the end of the 21st century for both, RCP4.5 and RCP8.5. The differences between RCP4.5 and RCP8.5 can be traced back to the mean and maximum duration of PAEs. At the end of the 21st century, under consideration of RCP8.5 (RCP4.5) the mean duration of PAEs is 5.5 (2.0) times higher than within the historical period. With respect to RCP8.5, the maximum duration of PAEs at the end of the 21st century is longer than a month (35.5 days), whereas the maximum duration of RCP4.5 is 14.3 days.

4.3.3. Heat events

Similar, although less distinct trends, can be observed for HDs and HEs (Fig. 8). On average, in the historical period only one day per year is by definition an HD and an HE approximately occurs every two years. Most of the HEs exhibit a duration of 1–2 days and heat events of ten or more days exhibit a return rate of 100 years. Even under consideration of RCP4.5, HEs of more than 10 days are unlikely at the end of the 21st century, although the return rate decreases by a factor of 10. In contrast, HEs of less than 5 days are very likely since one or more HEs of 1–2 days will occur each year, and the appearance of a small HW in three out of four years seems to be more than likely. For RCP8.5, especially HDs where TMAX exceeds the threshold increase significantly. At the end of the 21st century, more than 33 days are by definition HDs (Fig. 9) and more than three HEs of 1–2 days as well as up to two HEs of 3–5 days per year seem to be likely. Furthermore, under consideration of RCP8.5, the likelihood of large HWs in the period 2070–2100 is higher than the likelihood for small HWs in RCP4.5 for the same period (Fig. 8).

In Fig. 8, the heat day period (HDP) is depicted at the bottom. It shows that the HDP of the historical period is mainly located in the last third of July and lasts 10–11 days. More than 20 years do not exhibit an HD at all. Under consideration of RCP4.5, an extension of the HDP takes place especially due to an earlier start of the HDP. In the early 21st century, the HDP starts 9 days earlier whereas the end of the HDP is only 3 days earlier than within the historical period. In the middle of the 21st century, the start of the HDP remains almost constant but the end is shifted to the early third of August. Thus, the HDP lasts 30 days and only 6 years do not exhibit a heat day. A further extension of the HDP can be identified at the end of the 21st century. Here, the HDP starts on July, 6th and ends on August, 14th. Thus, the HDP lasts 40 days and only three years do not exhibit an HD. A more alarming development can be identified for RCP8.5. While the HDP remains almost constant until the early 21st century, the extension of the HDP increases rapidly during the second half. At the end of the 21st century, the HDP starts at June, 11th and ends at September, 2nd. Thus, the HDP lasts 84 days and HDs can be identified for all years of the period 2070–2100. With respect to the historical period, the HDP under consideration of

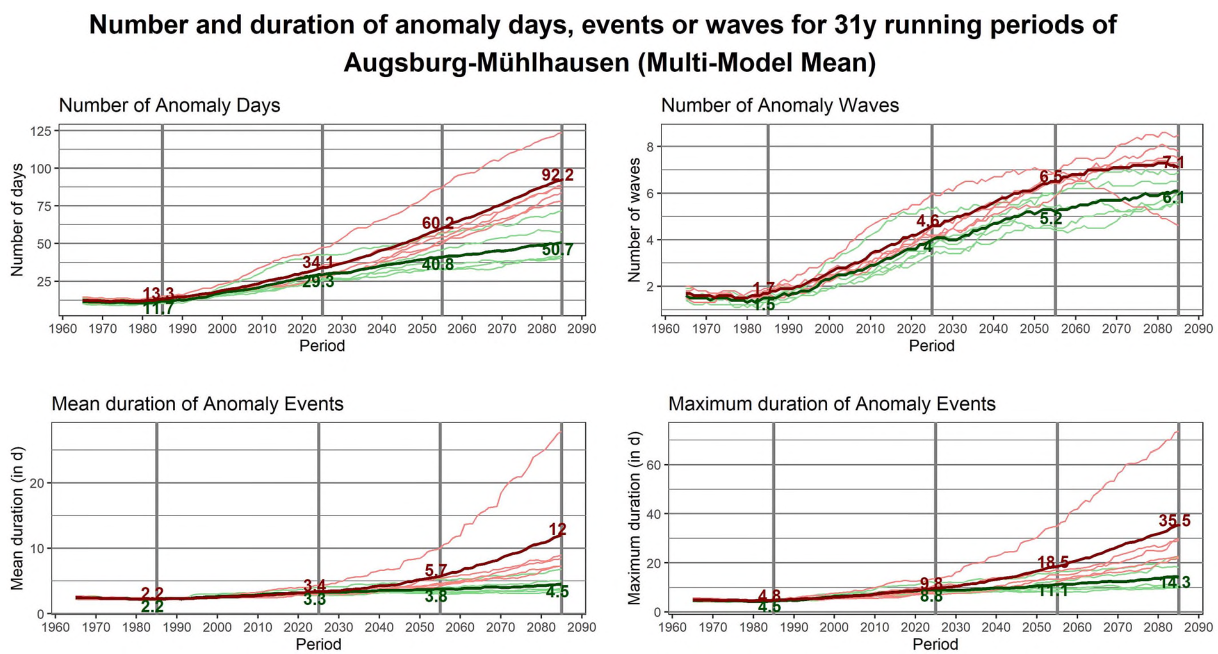

Fig. 7. Number of positive anomaly days and waves and duration of positive anomaly events for 31 year periods of Augsburg-Mühlhausen for RCP4.5 (green) and RCP8.5 (red). Vertical lines and associated numbers represent the historical reference period (1970–2000), the early (2010–2040), mid (2040–2070) and late (2070–2100) 21st century. Thin solid lines depict the time series of the GCMs, bold solid lines the time series for the multi-model mean. (For interpretation of the references to colour in this figure legend, the reader is referred to the web version of this article.)

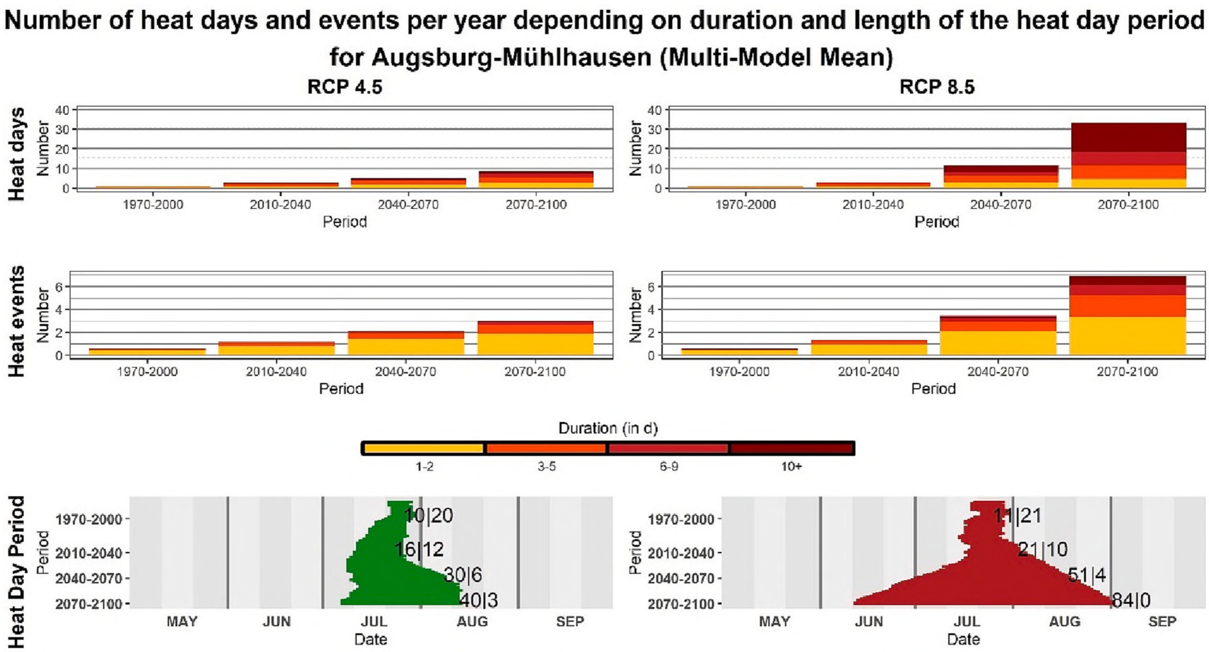

Fig. 8. Number of heat days (HDs, top) and events (HEs, middle) with respect to the length of an event for RCP4.5 (left) and RCP8.5 (right). Solid lines in the upper figures represent the absolute numbers, dashed lines the relative number in percent in steps of 10. The heat day period (bottom) represents the period between the first and last HD occurring within the extended summer season for 31 year running periods. The first numbers represent the mean duration of the heat day period and the second numbers the number of years without a heat day within the respective period (y-axis).

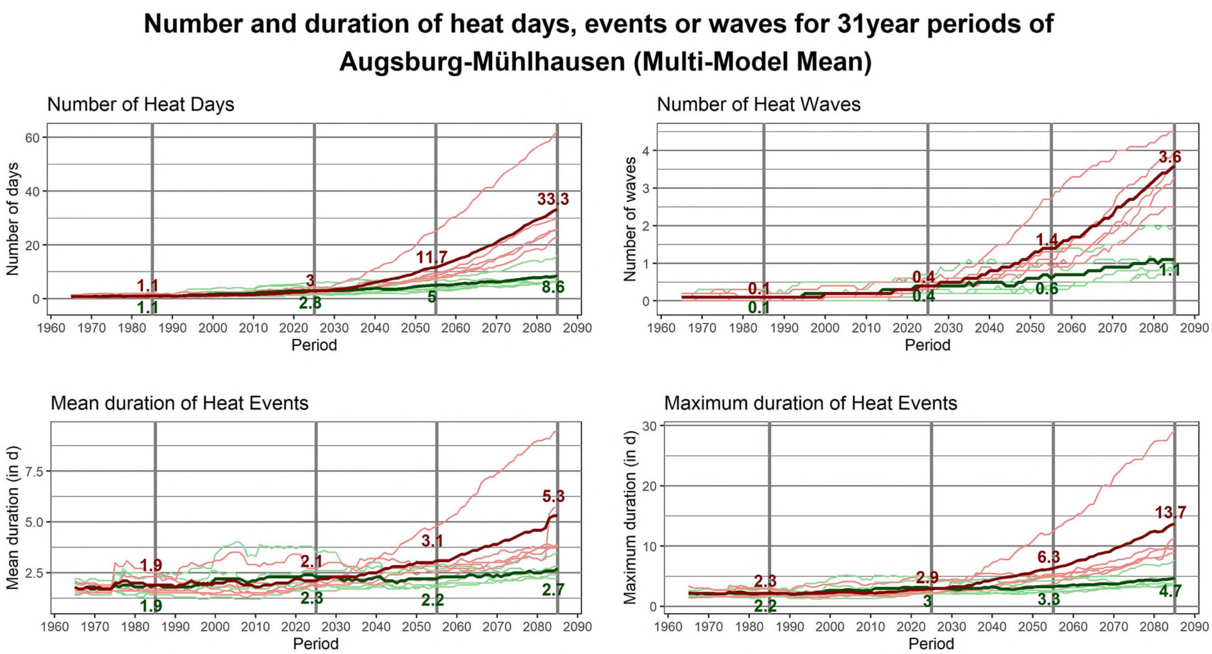

Fig. 9. Number of heat days and waves and duration of heat events for 31 year periods of Augsburg-Mühlhausen for RCP4.5 (green) and RCP8.5 (red). Vertical lines and associated numbers represent the historical reference period (1970–2000), the early (2010–2040), mid (2040–2070) and late (2070–2100) 21st century. Thin solid lines depict the time series of the GCMs, bold solid lines the time series for the multi-model mean. (For interpretation of the references to colour in this figure legend, the reader is referred to the web version of this article.)

RCP8.5 (RCP4.5) is 8 (4) times longer.

For RCP4.5, the mean and maximum duration of heat events (Fig. 9), show rather moderate changes until the end of the 21st century. The mean duration is prolonged by 0.8 days and maximum duration increases from 2.2 to 4.7. In contrast, in period 2070–2100, the mean duration of HEs under consideration of RCP8.5 is even higher than the maximum duration of RCP4.5. The mean duration is prolonged by 3.4 days, whereas the maximum duration is 13.7 days and, thus, 6 times higher than within the historical period.

4.4. Spatial projections for the city of Augsburg

4.4.1. Temperature

The spatial temperature distribution within the city of Augsburg for TMIN is presented in Fig. 10. Overall, only a small number of grid boxes (0.4%) exhibit a lower mean TMIN than the reference station Augsburg-Mühlhausen with highest values for the early 21st century, and subsequently decreasing numbers until the end of the 21st century. With respect to TMEAN, no grid box exhibits lower mean temperatures than the reference station within any period, whereas the mean of TMAX of approximately 2.3% grid boxes is lower. In order to determine the coldest (hottest) regions within the city of Augsburg, the 100 grid boxes with the lowest (highest) temperature values were assigned to the respective districts. The coldest regions of TMIN are settled in the North (Firnhaberau, Hammerschmiede) and South (Inningen, Göggingen-Süd) of Augsburg and the hottest regions are in the center of Augsburg, on the western (Bahnhofs- and Bismarckviertel, Innenstadt St. Ulrich Dom) and eastern side (Lechhausen-Süd) of the Lech River. The hottest regions for TMEAN are slightly shifted to the East (Innenstadt St. Ulrich Dom, Jakobervorstadt-Nord, Lechhausen Süd) whereas the coolest regions are settled in the southeastern (Siebenbrunn, Haunstetten-Süd) and -western parts (Bergheim) of the city. For TMAX, the coolest regions appear in the North (Firnhaberau, Hammerschmiede, Rechts der Wertach) and the hottest regions are settled in the western part of the city (Pfersee-Süd, Kriegshaber, Rosenau- Thelottviertel). The figures for TMEAN and TMAX corresponding to Fig. 10 are attached in S4.

The rates of temperature rise are rather the same for the coldest and hottest regions. This holds true both for RCP4.5 as well as RCP8.5 but with higher rates under consideration of RCP8.5. The greatest differences between hot and cold regions within the city of Augsburg occur for TMIN (3.8 °C) and lowest differences arise for TMEAN (1.9 °C). At the end of the 21st century the difference between RCP4.5 and RCP8.5 is lowest for TMIN (2.3 °C) and highest for TMAX (2.9 °C). Overall, the mean temperatures of TMIN for the period 2070–2100 reach 18.8 °C (16.6 °C) for RCP8.5 (RCP4.5) in the city center and 15.1 °C (12.8 °C) in the cooler regions. For TMAX, the hottest regions exhibit temperatures of 29.1 °C (26.2 °C) and 26.9 °C (24.1 °C) within the coldest regions.

4.4.2. Positive anomalies

In Fig. 11, the numbers of PADs within the city of Augsburg are depicted for different periods. In period 1970–2000, the lowest number of PADs occurs in the southern parts of Augsburg. Only 7% of days exceed two of three thresholds in the districts Inningen and

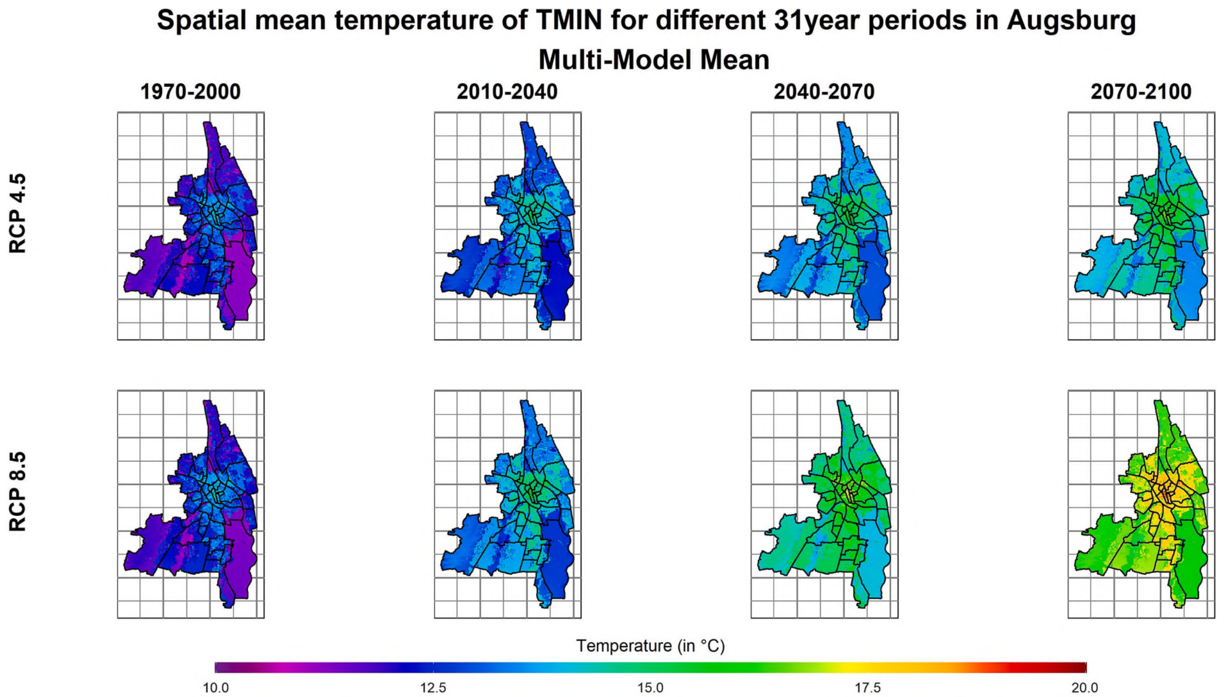

Fig. 10. Spatial mean temperatures of TMIN for different 31 year periods in Augsburg (columns) and RCPs (rows).

Göggingen-Süd. In contrast, over 30% of the days are by definition PADs within the wider range of the city center and in some parts of Lechhausen-Ost and the Rosenau- und Thelottviertel. At the end of the 21st century, the number of PADs increases to 57–71% (32–59%) under consideration of RCP8.5 (RCP4.5). Thus, the minimum number of PADs of RCP8.5 is almost as high as the maximum number for RCP4.5. Furthermore, for RCP8.5, the range of PADs within the city of Augsburg is already higher in period 2040–2070 than for RCP4.5 in period 2070–2100. The districts with minimum and maximum values rather remain the same, only the area of the cooler regions expands to the east (Haunstetten-Süd, Hochzoll-Süd and Siebenbrunn) under consideration of RCP8.5.

The increasing number of PADs leads to an increasing number of PAEs as well as an extension of mean and maximum duration (S 5). Within the reference period, the mean number of PAEs per year is between 1.2 and 6.8 events with a mean duration of 1.8–3.3 days, and maximum duration varies between 3.7 and 10.6 days. The area which is affected most frequently by PAEs is similar to the hottest region within the city of Augsburg. In contrast, the region with the lowest number of PAEs is additionally extended by regions in the northern edge of the city area. The hottest and coldest areas are also those regions where the longest or shortest PAEs took place.

Significant differences between RCP4.5 and RCP8.5 are projected from the period 2040–2070 onwards. Similar to the temperatures, mean and maximum duration of RCP4.5 within the period 2070–2100 are twice as low as under consideration of RCP8.5 and even lower than in period 2040–2070 of RCP8.5. In contrast, at the end of the 21st century the mean number of PAEs is higher for RCP4.5. At the end of the 21st century, for RCP8.5 (RCP4.5), PAEs of the city center last on average 14.7 (7.0) days and maximum events of over 43 (25) consecutive days are possible which is approximately 4 (2.5) times as high than within the reference period. Even the mean and maximum duration of the cooler regions are more than two times higher than in period 1970–2000.

4.4.3. Heat events

Within the reference period, a maximum number of 4% was determined as HD (Fig. 12). The area with the maximum number of HDs is located in the city center and, with growing distance to the center, the number is decreasing. Overall, a HE occurs in the cooler regions every 10 years and every two years in the hotter regions (S 6). When a HE occurs, the mean duration is 1.6–2.5 days and the maximum duration is 1.9–3.5 days. For the early 21st century, the number of HDs increases by 3–11% (3–9%) under consideration of RCP8.5 (RCP4.5), although the mean duration of HEs increases only slightly and both RCPs are rather on the same level. RCP4.5 and RCP8.5 also exhibit similar values for the maximum duration but, especially in the hotter regions, on a significantly higher level than within the reference period. Thus, differences between RCP4.5 and RCP8.5 can be traced back to a significant change of the recurrence interval of HEs. The recurrence interval for cooler regions decreases from 10 to 3.3 (5) years for RCP8.5 (RCP4.5) and in the hotter regions 2.2 (1.6) HEs will occur per year. At the end of the 21st century, the differences are highest with 6–18% HDs for RCP4.5 and 21–41% HDs for RCP8.5. Under consideration of RCP4.5, only one HE occurs per year during the extended summer season within the cooler regions and 3.6 per year in the hotter regions. The mean duration is 2–3.3 days and maximum duration is 3.8–9.4 days. In contrast, under consideration of RCP8.5, the number (3.7–6.5), mean (3.5–6.1) and maximum duration (10.7–21.1) of HEs is higher for the cooler regions than expected for the hottest regions under RCP4.5.

In Fig. 13, the HDP is displayed for each city district, depending on RCP and period. It shows, that the HDP within the reference period (dark colors) last from mid of July to the first third of August for the hotter districts or end of July, respectively, for the cooler districts. The HDP exhibit a maximum duration of 25 days for the district Innenstadt, St. Ullrich Dom, starting at July, 15th (July, 13th)

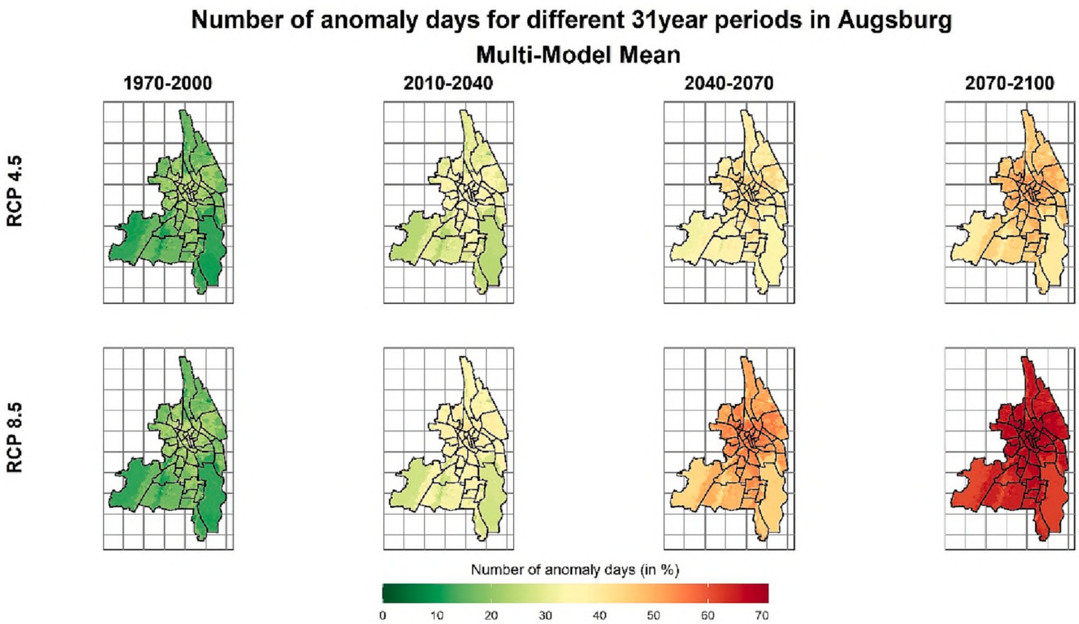

Fig. 11. Number of positive anomaly days for different 31 year periods (columns) and RCPs (rows) in Augsburg.

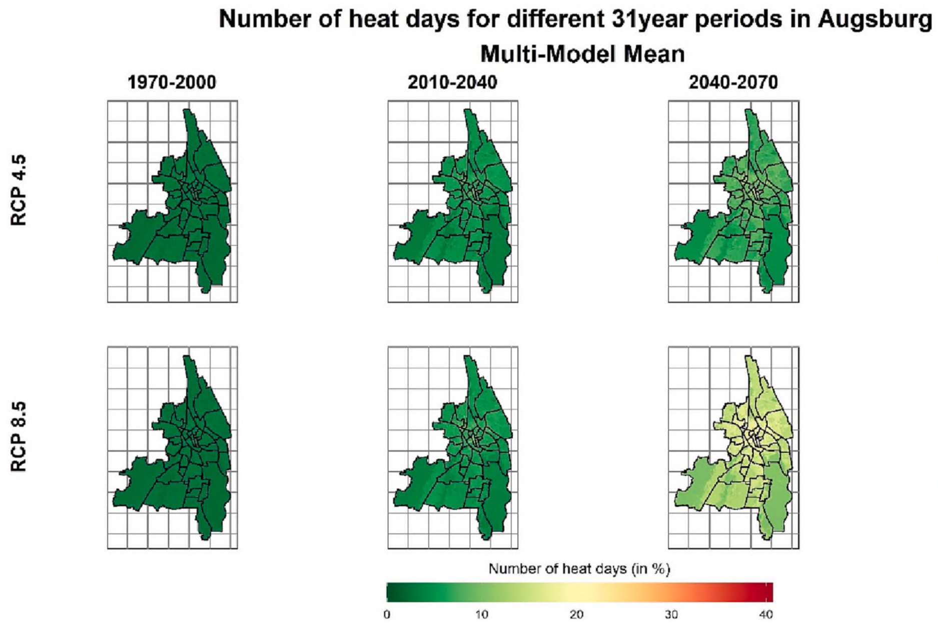

Fig. 12. Number of heat days for different 31 year periods (columns) and RCPs (rows) in Augsburg.

and ending at August, 8th (August, 6th) under consideration of RCP4.5 (RCP8.5). Thus, the duration of the HDP of the city center is more than twice as high than the HDP of Siebenbrunn which represents the district with the shortest HDP (12 days, July, 19th – July, 30th). Overall, the mean duration of the HDP within the reference period is 17.0 days. The districts of the city center exhibit a HDP of 20.7 which is, on average, 6 days longer than the HDP within the districts at the periphery of the city. In period 2010–2040, the mean duration of the HDP increases significantly for both RCPs but with higher rates for RCP8.5. The mean duration of the HDP is 25.0 (21.4) days longer for RCP8.5 (RCP4.5) and, thus, more than twice as high as within the reference period. For both RCPs, the rate of increase

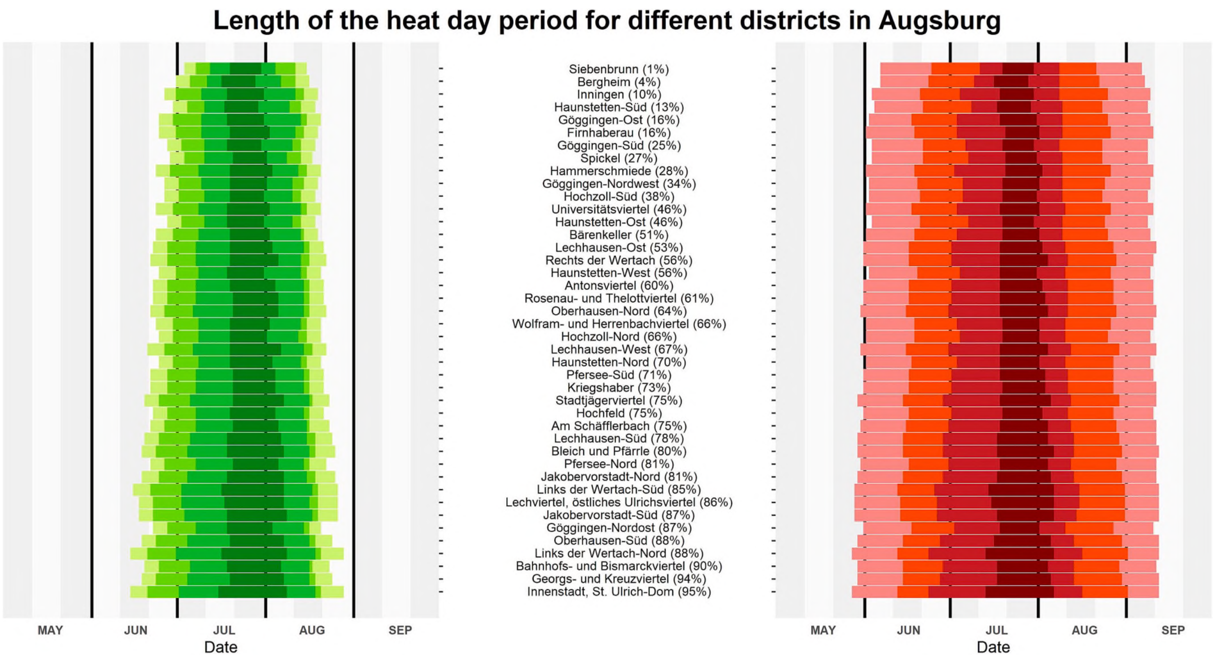

Fig. 13. Length of the heat day period by district within the city of Augsburg for different 31 year periods (from dark to light colors: 1970–2000, 2010–2040, 2040–2070, 2070–2100) under consideration of RCP4.5 (left, green) and RCP8.5 (right, red). The districts are ordered from top (low) to bottom (high) according to the fraction of sealed areas (percentage in brackets). (For interpretation of the references to colour in this figure legend, the reader is referred to the web version of this article.)

is strongest in the center of the city and decreasing rates towards the outskirts. In comparison with RCP8.5, the HDP of RCP4.5 is postponed. Thus, the HDP starts five days later, and ends two days later. On average, the HDP in the center of the city is 10 days longer than it is projected for the periphery of the city with maximum differences of 26 days between Siebenbrunn (RCP4.5: 24; RCP8.5: 29) and Links der Wertach Nord (50; 55). In period 2040–2070, differing trends are projected for RCP4.5 and RCP8.5. While the rate of increase under consideration of RCP4.5 is 9.4 days lower than in the early 21st century, the rate increases by 5.7 for RCP8.5. Thus, the mean duration of the HDP is 21.9 days longer for RCP8.5 (72.4) than for RCP4.5 (50.5). The difference between the rates of the city center and the outskirts is significantly smaller (RCP4.5) or inverted (RCP8.5), respectively. This means that under consideration of RCP8.5, from the middle of the 21st century, the extension of the HDP is progressing faster in the outskirts than in the city center. The same development is also projected for the end of the 21st century with a rate of increase which is 3.4 higher for the outskirts. Thus, with respect to the length of the HDP, an assimilation between city center and outskirts is projected, whereas the difference steadily grows for RCP4.5. On average, the HDP of RCP8.5 (102.9) is twice as high than the HDP of RCP4.5 (61.3). The districts Links der Wertach Nord and Innenstadt, St. Ulrich Dom exhibit maximum lengths of 109 days (RCP8.5) and a minimum length of 44 days (RCP4.5) is projected for Siebenbrunn. Thus, the longest HDP starts on May, 27th and ends September, 12th whereas the shortest HDP starts on July, 3rd and ends August, 15th.

5. Discussion

5.1. Model setup and skill

The present study shows a method for high-resolution intra-urban temperature assessments solely based on statistical methods. The downscaling of large-scale information was performed by means of a novel analog method which can keep up with existing methods (e.g., Zorita and Von Storch, 1999) but with the advantage of less computational time due to reduced input data required (Merkenschlager et al., 2021). The spatial projection of temperatures is based on a Multiple Linear Regression (MLR) which takes temporal and spatial predictor variables into account. Furthermore, the present approach tries to capture the urban heat island effect not only by a single center but by multiple so-called urban agglomeration centers. The UACs were derived by a cluster analysis and weighted distances were calculated under consideration of distance, relative position of logger or grid box to the center as well as wind speed and direction. MLR models were then established for all temperature variables and the leading four essential large-scale circulation patterns, separately. The described method provides assessments for temperatures of adequate skill. Improvements are still possible since the weighted distance model has not yet reached its full potential. For example, for high wind speeds, the UHI effect decreases but the weighted distances still increase. However, since intra-urban thermal differences can also be identified under disturbed conditions (Beck et al., 2018), the model was applied to the entire data set even if the effect is probably overestimated for stormy days. Furthermore, an elaborated model could also be adapted to other spatial variables. However, the consideration of the weighted distance model leads to an increase of skill and, thus, the method was taken into account for projections.

Model skill and the selection of predictor variables are depending on the respective temperature time series. In general, the higher the temperature difference between city center and environs, the higher the skill of the model. When the overall temperature variability within the city is higher, it is easier for the MLR model to establish relationships between explanatory and response variables. Thus, the highest model skill can be observed for TMIN since the UHI is most pronounced during night time (2.6 °C on average). Furthermore, the climate predictor variables can be divided into two groups: Predictors which indirectly describe incoming solar radiation (e.g., SD, CC) and predictors which indirectly describe the storage capacity of incoming solar radiation and evapotranspiration (e.g., RHUM, VAPOR). This is confirmed by Zhang et al. (2022) and references therein which describe evapotranspiration as one of the major drivers for the UHI effect. Depending on the temperature time series, either the one or the other is more significant. Since incoming solar radiation and related processes are negligible during night time, predictors like SD or CC are mainly removed from the final model for TMIN and variables representing thermodynamic (RHUM, VAPOR) processes are more important. Due to a higher heat storage capacity, humid air can absorb more heat and, thus, cooling rates during night-time are lower. In contrast, the predictor set of TMEAN contains more information about the incoming solar radiation and thermodynamic variables are eliminated. Since the temperature gradient between hottest and coolest region of the city is small for TMAX (0.6 °C on average), on the one hand model skill is relatively low and on the other hand, intra-urban temperature differences can hardly be assigned to specific predictors. Thus, the predictor set contains almost all climate variables since no variable was proofed to be non-significant.

With respect to the local-specific predictors, the SVF can also be attributed to the predictor group which indirectly describes heat storage capacity of incoming solar radiation. In this study, the SVF is solely based on buildings and, thus, the SVF provides information about building geometry (e.g., size, height, exterior surfaces). Since exterior walls exhibit the highest surface temperatures at night (Chudnovsky et al., 2004), the SVF also gives indications about how much longwave (shortwave) radiation can be emitted (absorbed) from the building during nighttime (daytime). During daytime, the UHI is significantly smaller due to the low-level atmospheric structure and strong mixing of the air by turbulence. Furthermore, the SVF and derived building geometry can counteract the UHI because of shadowing effects (Masson et al., 2020). However, since the UHI is significantly smaller during daytime and information on surface and the urban structure are also provided by UA and LCZ, the SVF is only considered in models were UA and/or LCZ are missing. Where UA and LCZ are considered as predictor, the SVF provides no additional important information for assessing TMEAN or TMAX. Although UA and LCZ contain similar information, both predictors are significant for most models whereas elevation hardly affects temperature assessments. This is due to the relatively small differences in altitude within the city of Augsburg. In contrast, temperature of Augsburg-Mühlhausen and circulation are the only predictors which are significant in each model. The most important UAC for all MLR models is UAC-7 located in the city center of Augsburg, since only one model eliminates these UAC. Overall, the consideration of UACs improves the model skill (MSESS +0.0914 on average) in comparison to models which do not consider UACs.

5.2. Reference period

Within the reference period, only TMIN shows significant differences between observations and reanalysis or GCMs. This could be traced back to trends with different signs between 2000 and 2006. The observation time series exhibits decreasing minimum temperatures but all models provide increasing minimum temperatures for the period 2000–2006. Analysis have shown that, due to land use changes in the nearby vicinity of Augsburg-Mühlhausen weather station, the minimum temperature time series is affected by inhomogeneous behavior. Gravel extraction leads to a lower groundwater level and, thus, to a loss of soil humidity which predominantly affects heat storage capacity and, thus, processes during nighttime (Merkenschlager et al., 2021). In contrast, for the reference period, the temperature time series of TMEAN and TMAX are well represented by the different models.

5.3. Projections

For projections it is conspicuous that the Australian model is very different in comparison to the other models. The projected number of heat and anomaly days or events by far exceeds the projected number of the other models. But since the distribution of the predictor variables within the historical period as well as the trend of the seasonal temperatures corresponds to the other models, ACCESS1.0 is yet taken into account for projections. However, indications about different behavior within the reference period of ACCESS1.0 can be derived from the heat season. It seems that heat relevant processes occur earlier within the year and, thus, the expansion of the heat season during the 21st century is faster. Further analyses are necessary to provide more information about the processes which are responsible for the temperature behavior of ACCESS1.0.

The projections for the early 21st century hardly show a difference between RCP4.5 and RCP8.5 since mitigation actions do not produce discernibly different climate change outcomes within the early years (IPCC, 2013). Thus, effects on the local climate of Augsburg rather remain the same, independent of the underlying emission scenario. The only difference between both RCPs is that the rate of increase is highest for RCP4.5 but lowest for RCP8.5. With respect to anomaly events, an increasing number of ADs results in longer and more frequent occurrence of anomaly events. The same situation can also be observed for heat events. From the mid-21st century on, the differences between both RCPs become obvious and increase steadily until the end of the 21st century. The significantly higher number of anomaly days in the period 2070–2100 under consideration of RCP8.5 results in a reduction of events since recovery periods between events disappear and former short events are merged to one longer lasting event. Thus, the mean and maximum duration of events for RCP8.5 is almost doubled with respect to the mid-21st century. For heat events, this effect has not yet taken place but the number of heat days at the end of the 21st century is more than 30 times higher than within the reference period and, thus, significantly higher than projected for anomaly days (7 times higher). Furthermore, a heat event within the reference period occurs every ten years with a mean duration of approximately 2 days. At the end of the 21st century, events with a mean duration of more than 5 days occur more than three times a year. In comparison, at the end of the 21st century, the duration and number of heat events under consideration of RCP4.5 is also higher than within the reference period but, here, only one event with a mean duration of less than three days per year is projected.

With respect to circulation patterns, the relative frequency remains almost constant through the 21st century. Only with respect to the relative frequency of circulation patterns on PADs, a shift takes place. The fraction of the positive mode of PC-2 increases in favor of the positive mode of PC-1. This is remarkable since the positive mode of PC-2 is characterized by winds from northwestern directions. This leads to the assumption that global warming leads to a general warming of air masses advected over the northern Atlantic so that former cooler weather conditions are increasingly able to exceed the relative temperature thresholds in Augsburg.

5.4. Intra-urban assessments of heat events

In general, the spatial temperature assessments show higher temperatures and more and longer heat events for areas near the city center and decreasing values towards the periphery. For TMIN and TMEAN, the region of the hottest districts remains almost the same (city center, Lechhausen-Süd). In contrast, the hottest regions of TMAX represent districts within the western part of the urban area. All districts are characterized by a small fraction of green space and a high fraction of sealed areas. Differences between the city center and the districts in the western part of the city are that in the center the buildings are significantly higher and, thus, the SVF is lower. The emission of thermal radiation at night and shadowing effects during day time are one reason why temperatures are highest for TMIN and TMEAN and slightly smaller for TMAX with respect to the western city districts. Furthermore, the western districts are located within a relatively small topographic sink so that air masses can heat up on calm days. Due to the western exposure and low buildings, solar radiation can unhamperedly heat up the air within the districts at the afternoon when temperatures reach their maximum. Thus, maximum temperatures of the western districts are higher than within the city center. The cooler districts are unexceptionally located at the periphery and are generally characterized by a high fraction of green space, a sparse development and, to some extent, a relatively high fraction of water bodies. With respect to TMIN, the cooler districts mainly exhibit agricultural land and a low fraction of forested areas. A low fraction of trees is essential for cooling during night time since surface are above normal under the tree canopy (Chudnovsky et al., 2004). The tree canopy behaves like a trap for long-wave terrestrial radiation (Ziter et al., 2019). In contrast, districts with vast forests exhibit the lowest mean temperatures within the city borders of Augsburg. Since tree shade can result in reduction of short-wave radiation reaching the surface by 60–90% (Winbourne et al., 2020), the surface temperature difference between shaded and sunny areas can exceed 20 °C (Rahman et al., 2020) and also air temperature is substantially lower. Due to evapotranspiration of trees the cooling effect is reinforced within forested areas (Jusuf et al., 2007). Furthermore, a large number of water bodies as well as the proximity to the Lech River provide additional cooling in the southeastern parts of the city. But large forested areas also hamper the exchange of air masses since they exhibit a high friction which decelerates air stream on windy days. Overall, forested areas exhibit a balancing effect with low mean temperatures and low temperature variability. In contrast, low developed areas with a high fraction of agricultural areas with low plants exhibit a high temperature variability since they can heat up fast on warm and calm days and cool down fast on cooler and windy days. When two rivers cross these areas which have their headwater in the alpine region, an additional cooling effect is available. Thus, the coldest regions with respect to TMAX are located in the north of Augsburg in the confluence of Lech and Wertach and surrounding areas.

The projected climate change leads not only to an increase in number and duration of events but also to more areas within the city which have to deal with extreme events. While some districts get off relatively lightly with respect to heat events or anomaly events under consideration of RCP4.5, the differences between hot and cool areas within the city slowly disappear under consideration of RCP8.5. For RCP4.5, the difference between hot and cool areas with respect to the length of the heat day period is more than a month, whereas the difference for RCP8.5 only amounts to 16 days. This is particularly noticeable for the number of days and events since, under consideration of RCP4.5, the cool areas within the city of Augsburg are only half as often affected by heat days or events than the hot regions. In contrast, the difference in number of heat days and events for RCP8.5 is only 25%. This is due to the fact that the missing green space, a high fraction of sealed areas and the heat storage capacity of the buildings within the city center favor the urban heat island effect during night-time. Thus, especially TMIN exceeds regularly the absolute temperature threshold within the city center leading to a significant higher number of heat days.

6. Conclusion

The present study provides assessments of high-resolution temperature and heat extremes within the city of Augsburg for two different RCPs (until 2100). The applied downscaling approach obtains similar skills in comparison to an established analog approach but with less computational costs. Results have shown that it does matter if we achieve the 2 °C target (similar to RCP4.5) since urban greening or other adaption policies can only mitigate and not counteract the impacts of climate change within urban areas. This is shown by the fact that, with the exception of TMIN, the temperature difference between both scenarios is far greater than between cool and hot regions within the city of Augsburg. Overall, the temperature difference between hot and cool regions of Augsburg is similar between both scenarios for all periods. Thus, no region within the city of Augsburg faces a significantly stronger or weaker temperature increase due to the underlying scenario. In contrast, with respect to heat waves, days and heat day period, differences between hot and cool regions as well as the underlying scenarios are significant. All indices increase more sharply under RCP8.5 and, with the exception of the heat day period, within the warmer regions of the city.

But nevertheless, due to the assumption that the number of people which live in cities will increase and an ageing population is expected for Germany, it is of utmost importance to identify the climate hot spot regions within urban areas. On that basis and under consideration of socio-economic factors, urban planners obtain indications about the priority of structural modifications within the urban area. Furthermore, where intra-urban climate hotspots meet an inconvenient combination of socio-economic factors (e.g., elderly + living alone + socially deprived), public health services should provide special offers like warning systems or a dense medical care. Thus, the number of death and the number of people who suffer from heat can be reduced to a reasonable level.

CRediT authorship contribution statement

Christian Merkenschlager: Conceptualization, Methodology, Software, Validation, Formal analysis, Investigation, Writing – original draft, Writing – review & editing, Visualization. **Elke Hertig:** Supervision, Project administration, Funding acquisition, Conceptualization, Methodology. **Jonathan Simon:** Software, Formal analysis, Investigation. **Christoph Beck:** Supervision, Project administration, Funding acquisition, Conceptualization, Data curation, Resources.

Declaration of Competing Interest

The authors declare that they have no known competing financial interests or personal relationships that could have appeared to influence the work reported in this paper.

Data availability

Data will be made available on request.

Acknowledgements

This study was funded by Deutsche Forschungsgemeinschaft (DFG, German Research Foundation) under project HE6186/5-1 and under project number 408057478 as well as under project BE 2406/3-1.

References

Amt für Statistik und Stadforschung, Stadt Augsburg, 2017. Statistisches Jahrbuch 2017 - Ein Einblick. Abgerufen am 6. 6 2021 von. www.augsburg.de.

Bartos, M., Chester, M., 2014. Assessing Future Extreme Heat Events at Intra-Urban Scales: A Comparative Study of Phoenix and Los Angeles.

Bechtel, B., Daneke, C., 2012. Classification of local climate zones based on multiple earth observation data. IEEE Journal of Selected Topics in Applied Earth Observations and Remote Sensing 5 (4), 1191–1202.

Bechtel, B., Alexander, P.J., Böhner, J., Ching, J., Conrad, O., Feddema, J., et al., 2015. Mapping local climate zones for a worldwide database of the form and function of cities. ISPRS Int. J. Geo Inf. 4 (1), 199–219.

Beck, C., Straub, A., Breitner, S., Cyrys, J., Philipp, A., Rathmann, J., et al., 2018. Air temperature characteristics of local climate zones in the Augsburg urban area (Bavaria, southern Germany) under varying synoptic conditions. Urban Clim. 25, 152–166.

Brands, S.H., 2013. How well do CMIP5 earth system models simulate present climate conditions in Europe and Africa? Clim. Dyn. 41 (3–4), 803–817.

Bueno, B., Norford, L., Hidalgo, J., Pigeon, G., 2013. The urban weather generator. J. Build. Perform. Simul. 6 (4), 269–281.

Cheng, Y., 1995. Mean shift, mode seeking, and clustering. IEEE Trans. Pattern Anal. Mach. Intell. 17 (8), 790–799.

Chudnovsky, A., Ben-Dor, E., Saaroni, H., 2004. Diurnal thermal behavior of selected urban objects using remote sensing measurements. Energy and Buildings 36 (11), 1063–1074.

Copernicus Climate Change Service (C3S), 2017. ERA5: Fifth generation of ECMWF atmospheric reanalyses of the global climate. Von Copernicus Climate Change Service Climate Data Store (CDS). https://cds.climate.copernicus.eu/cdsapp#!/homeabgerufen.

Diaz-Nieto, J., Wilby, R.L., 2005. A comparison of statistical downscaling and climate change factor methods: impacts on low flows in the river Thames, United Kingdom. Clim. Chang. 69 (2), 245–268.

DWD Climate Data Center Deutscher Wetterdienst, 2019. Hourly mean values of air temperature, wind speed and cloudiness for Augsburg- Mühlhausen. Abgerufen am 14. 8 2019 von. http://www.dwd.de.

EEA (European Environment Agency), 2010. Urban Atlas. Kopenhagen.

Fischer, E.M., Schär, C., 2010. Consistent geographical patterns of changes in high-impact European heatwaves. Nat. Geosci. 3 (6), 398–403.

Gutierrez, J., San-Martin, D., Brands, S., Manzanas, R.H., 2013. Reassessing statistical downscaling techniques for their robust application under climate change conditions. J. Clim. 26 (1), 171–188.

Hamdi, R., Van de Vyver, H., De Troch, R., Termonia, P., 2014. Assessment of three dynamical urban climate downscaling methods: Brussels's future urban heat island under an A1B emission scenario. Int. J. Climatol. 34 (4), 978–999.

Hertig, E., Jacobeit, J., 2008. Assessments of Mediterranean precipitation changes for the 21st century using statistical downscaling techniques. Int. J. Climatol. 28 (8), 1025–1045.

Ho, H.C., Knudby, A., Sirovyak, P., Xu, Y., Hodul, M., Henderson, S.B., 2014. Mapping maximum urban air temperature on hot summer days. Remote Sens. Environ. 154, 38–45.

Howard, L., 1818. The Climate of London: Deduced from Meteorological Observations, Made at Different Places in the Neighbourhood of the Metropolis. vol. 1. Picadilly: W. Phillips, George Yard, Lombard Street, sold also by J. and A. Arch, Cornhill; Baldwin, Cradock, and W. Bent, Paternoster Row; and J. Hatchard, Picadilly.

IPCC, 2013. In: Stocker, T., Qin, D., Plattner, G.-K., Tignor, M., Allen, S.K., Boschung, J., et al. (Eds.), Climate Change 2013: The Physical Science Basis. Contribution of Working Group I to the Fifth Assessment Report of the Intergovernmental Panel on Climate Change. Cambridge University Press, Cambridge, United Kingdom and New York, NY, USA.

IPCC, 2021. Summary for policymakers. In: Masson-Delmotte, V., Zhai, P., Connors, S., Péan, C., Berger, S., et al. (Eds.), Climate Change 2021: The Physical Science Basis. Contribution of Working Group I to the Sixth Assessment Report of the Intergovernmental Panel on Climate Change. Cambridge University Press, Cambridge, United Kingdom and New York, NY, USA, pp. 3–32.

Jusuf, S.K., Wong, N.H., Hagen, E., Anggoro, R., Hong, Y., 2007. The influence of land use on the urban heat island in. Singapore. 31 (2), 232–242.

Ketterer, C., Matzarakis, A., 2015. Comparison of different methods for the assessment of the urban heat island in Stuttgart, Germany. Int. J. Biometeorol. 59 (9), 1299–1309.

Kilbourne, E., 1997. Heat waves and hot environments. In: Noji, E. (Ed.), The public health consequences of disasters. Oxford Univ. press, New York.

Kottek, M., Grieser, J., Beck, C., Rudolf, B., Rubel, F., 2006. World map of the Köppen-Geiger climate classification updated. Meteorol. Z. 15 (3), 259–263.

Kovats, R., Hajat, S., 2008. Heat stress and public health: a critical review. Annu. Rev. Public Health 29, 41–55.

Lauwaet, D., De Ridder, K., Saeed, S., Brisson, E., Chatterjee, F., van Lipzig, N.P., et al., 2016. Assessing the current and future urban heat island of Brussels. Urban Clim. 15, 1–15.

LDBV, 2017. Landesamt für Digitalisierung, Breitband und Vermessung. Abgerufen am 9. 7 2017 von. https://www.ldbv.bayern.de/.

Le Bras, J., Masson, V., 2015. A fast and spatialized urban weather generator for long-term urban studies at the city-scale. Front. Earth Sci. 3, 27.

Makido, Y., Ferwati, S., Sailor, D., 2016. Daytime variation of urban heat islands: the case study of Doha, Qatar. Climate 4 (2), 32.

Masson, V., Lemonsu, A., Hidalgo, J., Voogt, J., 2020. Urban climates and climate change. Annu. Rev. Environ. Resour. 45, 411–444.

Meehl, G.A., Tebaldi, C., 2004. More intense, more frequent, and longer lasting heat waves in the 21st century. Science 305 (5686), 994–997.

Merkenschlager, C., Koller, S., Beck, C., Hertig, E., 2021. Assessing local daily temperatures by means of novel analog approaches: a case study based on the city of Augsburg, Germany. Theor. Appl. Climatol. 145 (1), 31–46.

Oke, T., 1987. *Boundary Layer Climates* (2. Ausg.). Routledge, London, New York.

Oke, T.R., Mills, G., Christen, A., Voogt, J.A., 2017. Urban climates. University Press, Camebridge.

Onset, 2010. HOBO Pro v2 (U23-00x) Manual. Abgerufen am 9. 1 2018 von. http://www.onsetcomp.com/files/manual_pdfs/10694-P%20MAN-U23.pdf.

Ortiz, L.E., González, J.E., Horton, R., Lin, W., Wu, W., Ramamurthy, P., et al., 2019. High-resolution projections of extreme heat in new York City. Int. J. Climatol. 39 (12) (4721–4635).

Pantavou, K., Theoharatos, G., Nikolopoulos, G., Katavoutas, G., Asimakopoulos, D., 2008. Pantavou, K., Theoharatos, G., NikoEvaluation of thermal discomfort in Athens territory and its effect on the daily number of recorded patients at hospitals' emergency rooms. Int. J. Biometeorol. 52 (8), 773–778.

Perkins, S.E., 2015. A review on the scientific understanding of heatwaves—their measurement, driving mechanism and changes at the global scale. Atmos. Res. 164, 242–267.

Preisendorfer, R., 1988. Principal component analysis in meteorology and oceanography (Bd. 425). (C. Mobeley, Hrsg.). Elsevier, Amsterdam.

Rahman, M.A., Stratopoulos, L.M., Moser-Reischl, A., Zölch, T., Häberle, K.H., Rötzer, T., et al., 2020. Traits of trees for cooling urban heat islands: a meta-analysis. Build. Environ. 170, 106606.

Rizwan, A.M., Dennis, L.Y., Chunho, L.I., 2008. A review on the generation, determination and mitigation of urban Heat Island. J. Environ. Sci. 20 (1), 120–128.

Salvati, A., Palme, M., Inostroza, L., 2017. Key parameters for urban heat island assessment in a Mediterranean context: a sensitivity analysis using the urban weather generator model. In: IOP conference series: materials science and engineering, 245, p. 082055 no. 8.

Straub, A., Berger, K., Breitner, S., Cyrys, J., Geruschkat, U., Jacobeit, J., et al., 2019. Statistical modelling of spatial patterns of the urban heat island intensity in the urban environment of Augsburg, Germany. Urban Clim. 29, 100491.
Teutschbein, C., Wetterhall, F., Seibert, J., 2011. Evaluation of different downscaling techniques for hydrological climate-change impact studies at the catchment scale. Clim. Dyn. 37 (9–10), 2087–2105.
Vautard, C., Gobiet, A., Jacob, D., Belda, M., Colette, A., Déqué, M., et al., 2013. The simulation of European heat waves from an ensemble of regional climate models within the EURO-CORDEX project. Clim. Dyn. 41 (9–10), 2555–2575.
Winbourne, J.B., Jones, T.S., Garvey, S.M., Harrison, J.L., Wang, L., Li, D., Hutyra, L.R., 2020. Tree transpiration and urban temperatures: current understanding, implications, and future research directions. BioScience 70 (7), 576–588.
Zhang, Z., Paschalis, A., Mijic, A., Meili, N., Manoli, G., van Reeuwijk, M., Fatichi, S., 2022. A mechanistic assessment of urban heat island intensities and drivers across climates. Urban Clim. 44, 101215.
Zhao, L., Oppenheimer, M., Zhu, Q., Baldwin, J., Ebi, K., Bou-Zeid, E., et al., 2018. Interactions between urban heat islands and heat waves. Environmental Research Letters 13 (3), 034003.
Ziter, C., Pedersen, E., Kucharik, C., Turner, M., 2019. Scale-dependent interactions between tree canopy cover and impervious surfaces reduce daytime urban heat during summer. Proceedings of the National Academy of science 15, 7575. M.
Zorita, E., Von Storch, H., 1999. The analog method as a simple statistical downscaling technique: comparison with more complicated methods. J. Clim. 12 (8), 2474–2489.